

Comparative Study Between Similarly Processed YBa₂Cu₃O_{7-x} Films with Y₂BaCuO₅ or BaSnO₃ Additions

C. V. Varanasi, J. Burke, L. Brunke, J.H. Lee, H. Wang, P.N. Barnes

Abstract: A special YBa₂Cu₃O_{7-x} (YBCO) target with a thin sector of second phase material, in this case either Y₂BaCuO₅ (Y211) or BaSnO₃ (BSO), was used to deposit YBCO films with non-layered nanoparticles on single crystal LaAlO₃ and biaxially textured Ni-5 at.% W substrates buffered with CeO₂ and YSZ layers (coated conductors). Although identical processing conditions were used, TEM images indicated that random Y211 nanoparticles in the case of YBCO+Y211, and evenly spaced BSO nanocolumns in the case of YBCO+BSO, form in the YBCO films. While YBCO plane buckling was observed at many places in the case of YBCO+Y211, a high density of stacking faults and dislocations were observed in the case of YBCO+BSO near the BSO columns. In transport critical current density (J_c) angular dependence measurements, the absence of nanocolumns in YBCO+Y211 films resulted in the absence of a peak at 0°, J_c ($H//c$), in J_c vs. θ plots, as compared to a clear peak at 0° observed in YBCO+BSO films with the nanocolumns. The in-field J_c measurements indicated small low-field J_c enhancements at 77 K in YBCO+Y211 films but more than an order of magnitude improvement in high-field J_c in YBCO+BSO films due to the differences in the microstructures.

Index Terms – BaSnO₃, Coated conductors, Flux pinning, Pulsed laser ablation, Y211

I. INTRODUCTION

Flux pinning enhancement in coated conductors is highly desirable for the applications in high magnetic fields and to improve the engineering current density (J_e) of the conductors [1]. Second phase additions during the growth of YBa₂Cu₃O_{7-x} (YBCO) are now widely studied by several groups as a means to enhance the critical current density (J_c). Various second phase particles such as Y₂BaCuO₅ (Y211) [2,3], Y₂O₃[4], BaZrO₃[5] and BaSnO₃ (BSO)[6] etc. have been investigated with good success in enhancing the J_c . Introduction of second phase particles in YBCO films grown by pulsed laser ablation was initially done by two methods a) using two different targets and alternatively switching them during the growth [2] or b) use a premixed target prepared with desired amounts of second phase material [5,7].

Manuscript received 19 August 2008. This work was supported by the AFOSR and the Propulsion Directorate of the AFRL.

C. V. Varanasi, J. Burke, L. Brunke are with the University of Dayton Research Institute, Dayton, OH and Air Force Research Laboratory, WPAFB, OH (e-mail:chakrapani.varanasi@wpafb.af.mil.)
J.H. Lee, H. Wang, are with Texas A&M University, College Station, TX, (email:wangh@mail.ece.tamu.edu)
P.N. Barnes is with the Air Force Research Laboratory, WPAFB, OH (email paul.barnes@wpafb.af.mil)

Recently a third approach that uses a second phase material sector on the YBCO target has been discussed using Y211 sector as an example [3]. Later, similar approaches have been used to introduce other materials such as yttria stabilized zirconia (YSZ) etc. into YBCO with good success [8]. Recently, BSO has been also introduced into YBCO by using the sector target approach which yielded YBCO+BSO films with very good J_c improvements, especially at high fields [6, 10]. However, a comparative study of YBCO films processed using a similar process and amounts but with different chemical composition materials is lacking in the literature. This kind of study is important to understand the composition-structure-property relationships in YBCO materials. In this paper magnetization J_c , angular dependence of transport J_c , and transmission electron microscope images of the cross-section of YBCO+Y211 are compared with the YBCO+BSO films processed by similar processing method and amounts. The observed angular dependence of the transport current measurements is discussed in the light of the microstructural differences between YBCO+Y211 and YBCO+BSO. Results on YBCO+Y211 films deposited on buffered metallic substrates are presented as opposed to the initial results of YBCO+Y211 on single crystal LaAlO₃ substrates that were reported earlier [3].

II. EXPERIMENTAL

All the YBCO films with Y211 or BSO additions were processed using pulsed laser ablation employing a sectored target approach. A Neocera chamber with Lambda Physik laser ($\lambda = 248$ nm) was used for the depositions. A 30° sector cut from a thin disk of either Y211 or BSO was attached to the top surface of a YBCO target and it is periodically ablated as the target is rotated during the deposition. The second phase particles (Y211 or BSO) are introduced (expected to be 15-20 at.%) into the growing YBCO film whenever the laser hits the sector. All the films were processed using the same conditions: a laser energy density of 2 J/cm², 4Hz repetition rate, substrate to target distance of 6 cm, a growth temperature of 780 °C and 300 mTorr of O₂ ambience. Films were grown to approximately 250 – 300 nm thickness on buffered metallic substrates (CeO₂/YSZ/CeO₂ buffers on bi-axially textured Ni-5 at.%W) as well as single crystal (100) LaAlO₃ (LAO). The films were then annealed in-situ in the chamber at 500 °C at 600 Torr of O₂ pressure for 30 min. before cooling down to room temperature.

All the scanning electron microscope images of the samples were taken using a SIRION high resolution scanning electron microscope. Cross-sectional and plan-view transmission

electron microscopy (TEM) studies on all samples on LAO, including high resolution TEM (HRTEM), were performed with a Philips CM200 analytical electron microscope with point-to-point resolution of 0.21 nm. All the TEM samples were prepared through a conventional TEM sample preparation routine including cutting, gluing, grinding, polishing and precision ion polishing. Focused ion beam cross-sections of YBCO+Y211 sample on metallic substrates were observed using a FEI microscope to characterize the interfaces and to determine the depth of the pores. Magnetization J_c was calculated from the hysteresis loops data generated using a Quantum Design PPMS vibrating sample magnetometer and using the Bean's model. Transport current density measurements were taken on bridged samples in applied magnetic fields using a four probe method. Angular dependence of transport J_c with the magnetic field orientation was compared for YBCO+BSO and YBCO+Y211 samples.

III. RESULTS AND DISCUSSION

Figure 1 shows a SEM plan view image of a YBCO+Y211 film deposited on coated conductor substrate. These films showed the presence of porosity similar to the YBCO+Y211 films deposited on LaAlO_3 substrates as reported earlier [3]. It is thought that the Y211 nanoparticles of sufficiently small size can contribute to the formation of the porosity similar to the contribution from the vicinal steps on the YBCO films grown on vicinal substrates as reported in the previous studies [11]. However, the YBCO+BSO films did not show a similar porosity, possibly due to the formation of nanocolumns as opposed to discrete nanoparticles seen in YBCO+Y211, as discussed later.

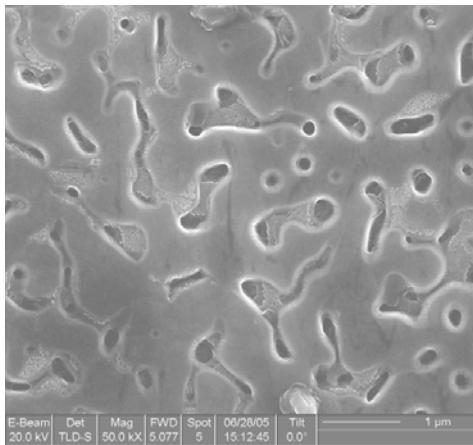


Fig. 1. Lower magnification image of the YBCO+Y211 coating on buffered metallic Ni-5 at.%W substrates.

A higher magnification SEM image is shown in Figure 2 where Y211 nanoparticles in the films can be clearly seen (bright white discrete particles as shown by arrows). Figure 3 shows the cross-sectional image of a coated conductor sample obtained by using a focused ion beam technique showing different layers present in the sample. All different layers of the buffers, namely CeO_2 , YSZ, and CeO_2 can be clearly seen. Some formation of NiWO_4 at the interface is observed in these

samples. The cross-sectional image shows that some of the pores can be very deep extending to more than half of the film thickness. This porosity is not necessarily undesirable as it can help in rapid oxygenation of the films. In addition it has been suggested that pores can also contribute to flux pinning via the surfaces [11].

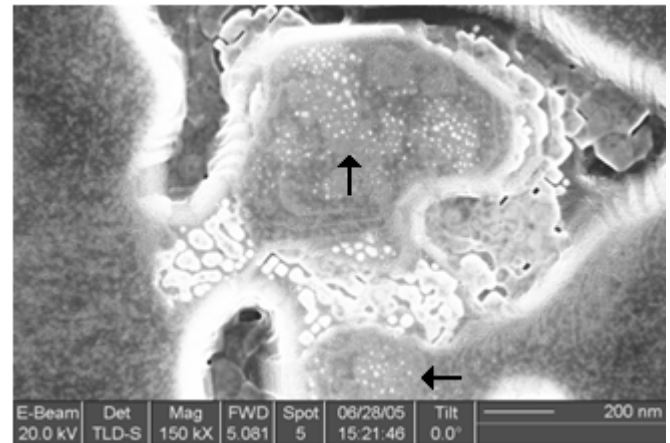


Fig. 2. High resolution secondary electron images of the YBCO+Y211 coatings on buffered metallic Ni-5at.%W substrates. Arrows show the nanoparticles.

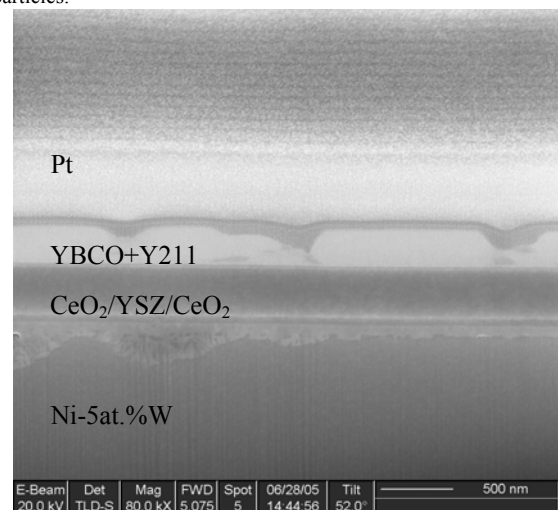


Fig. 3. Focused ion beam cross-sectional image of YBCO+Y211 coated conductor on Ni-5 at.%W

Figure 4 shows a TEM cross-sectional image of similarly processed YBCO+Y211 sample deposited on LaAlO_3 substrate where a number of Y211 particles can be seen as marked. It is estimated from this figure that, the average particle size is $4 \times 5 \text{ nm}$ (height \times width) and the particle density is $\sim 1 \times 10^{11} / \text{cm}^2$. If we assume the density is uniform throughout the sample thickness, the volume density is $\sim 2 \times 10^{16} / \text{cm}^3$. Figure 5 shows a high resolution image of YBCO+Y211 sample where extensive YBCO plane buckling was observed. It is believed that the buckling is partly caused by the presence of Y211 nanoparticles and compositional fluctuations. Figure 6 shows the cross-sectional TEM image of a similarly processed YBCO+BSO sample where evenly spaced BSO nanocolumns can be observed as opposed to discrete particles observed in the YBCO+Y211. In the YBCO+BSO samples, the rod density is estimated to be $\sim 3 \times 10^{11} / \text{cm}^2$. The average BSO nanorod size is about 7.5 nm .

In high resolution TEM, a high density of stacking faults and dislocations were noticed around these nanocolumns as reported elsewhere [9]. YBCO was observed to grow around the nanocolumns with good c-axis orientation.

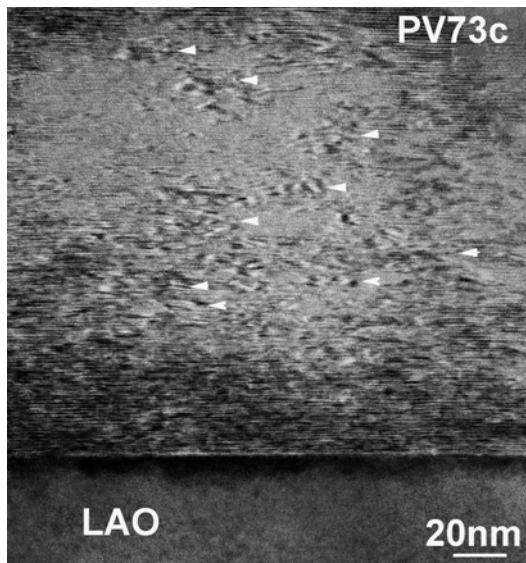


Fig. 4. Transmission Electron Microscope image of YBCO+Y211 sample deposited on LaAlO₃ substrates showing nanoparticles.

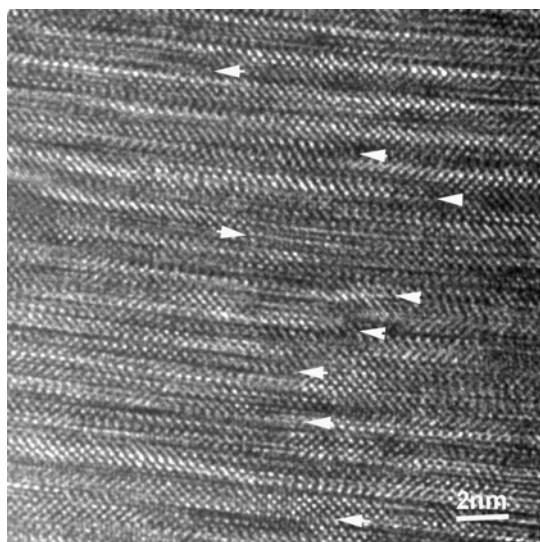


Fig. 5. High resolution Transmission Electron Microscope image showing YBCO plane buckling in YBCO+Y211 films deposited on LaAlO₃.

Figure 7 shows the magnetization J_c as a function of magnetic field of YBCO+Y211 and YBCO+BSO films at both 77 K and 65 K. YBCO+Y211 films seem to have slightly better J_c than YBCO+BSO at lower fields up to 2 T at 77 K. However, the YBCO+BSO samples show a much higher J_c at higher fields. More than an order of magnitude improvement in J_c was observed at the higher fields, e.g. at 6 T. As noted before (Figure 6), YBCO+BSO samples have nanocolumns perpendicular to the sample normal, or parallel to the c-axis. Since the magnetic field is applied parallel to the c-axis, the interaction between the flux lines and the nanocolumns is expected to be significant, resulting in higher flux pinning. Although YBCO+Y211 include nanoparticulates, the pinning

strength at high fields does not seem to be as significant. However, at lower fields, due to the lower density of flux lines and low Lorenz forces, the nanoparticulates could contribute to pinning. In addition, T_c of the films also may play a role in the J_c differences. It should be noted that the T_c of the films was found to be > 90 K for YBCO+Y211 films, but it is slightly depressed in the case of YBCO+BSO films to ~ 88 K. The T_c depression in YBCO+BSO (possibly due to Sn diffusion or strain due to nanocolumns in YBCO) is partly responsible for depressed J_c at lower fields in these films. At 65 K, the effect of the T_c difference is not as significant and so the YBCO+Y211 and YBCO+BSO samples appear to have similar J_c at low fields. However, at higher fields the improvements seem to occur in YBCO+BSO due to the nanocolumns as discussed before.

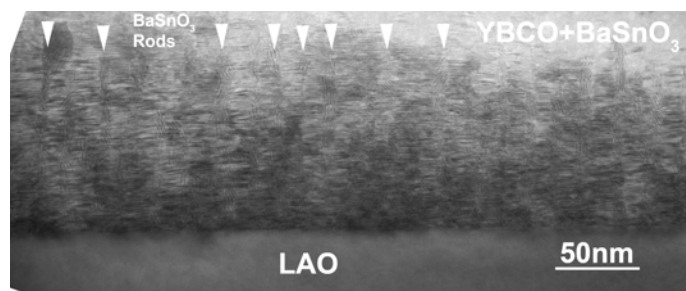


Fig. 6. BSO nanocolumns in a YBCO+BSO sample processed with a 30° BSO sector on a YBCO target on LaAlO₃ substrates.

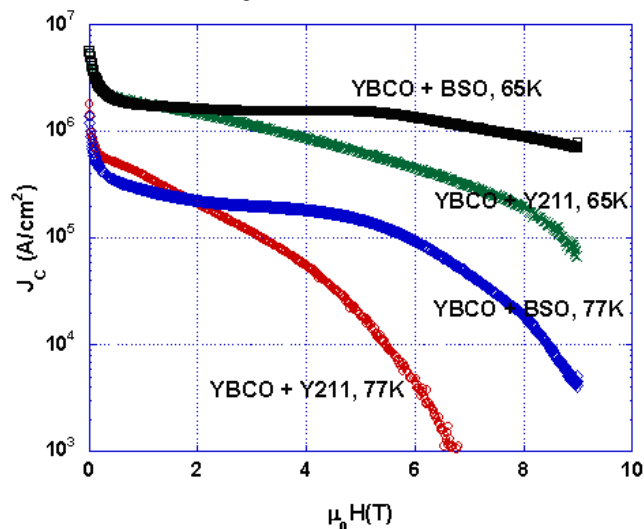


Fig. 7. Magnetization critical current density vs. the applied magnetic field of a YBCO+Y211 sample as compared to YBCO+BSO sample processed by similar method on LaAlO₃ substrates.

Figure 8 shows the transport J_c of YBCO+Y211 samples on a coated conductor substrate. A similar high J_c was noted as seen on single crystal LaAlO₃ substrates. The transport J_c was measured to be higher than the magnetization J_c as shown in Figure 7, consistent with the earlier observations. Figure 9 shows J_c vs. θ of YBCO+Y211 and YBCO+BSO coated conductor samples normalized to respective $J_c(H//ab)$ values. The YBCO+BSO clearly shows a peak at 0°, as compared to YBCO+Y211 that shows a relatively flat region, again confirming the contributions from the nanocolumns in YBCO+BSO and lack thereof in YBCO+Y211.

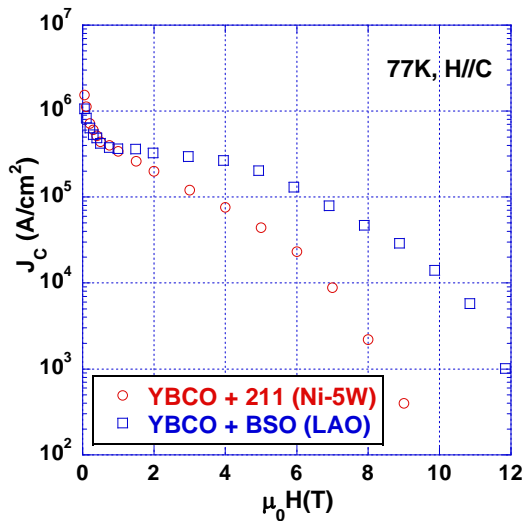


Fig. 8. Transport critical current density vs. the applied magnetic field of a YBCO+Y211 coated conductor sample.

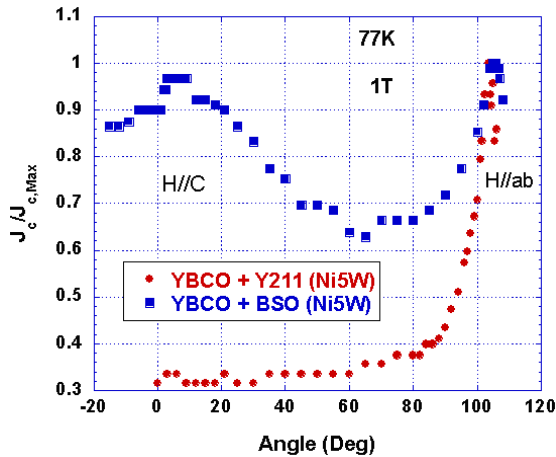


Fig. 9. Comparison of J_c angular dependence at 1 T for YBCO+Y211 and YBCO+BSO films on metallic substrates. Absence of peak in H//c can be clearly seen in YBCO+Y211 samples due to lack of nanocolumns.

Although both Y211 and BSO have a lattice mismatch with YBCO (for Y211 $\sim 7\%$ and for BSO it is 7.7%), the cubic perovskite structure of BSO is evidently important to form the nanocolumns in YBCO. Other examples of nanocolumn formation such as BZO [12] also seem to corroborate well with the present observations. However, it should also be noted that the growth of nanocolumns will depend on the processing conditions. While both Y211 and BSO were introduced into YBCO films in almost similar amounts by a similar method, Y211 forms the nanoparticles and BSO forms nanocolumns, likely caused by the suitable strain induced by the cubic perovskite structure of the BSO [13]. It is also interesting to note that although high volume fractions of the second phase are introduced, there is minimal degradation in the biaxial texture of YBCO films, suggesting that the growth of YBCO is less influenced by these additions. The presence of nanocolumns seems to be essential for the observed enhancements at high fields.

IV. CONCLUSIONS

In conclusion, it is shown that YBCO+Y211 films show J_c improvements over YBCO+BSO only at low magnetic fields at 77K. YBCO+BSO films show more than an order of magnitude improvement in J_c at high fields as compared to the YBCO+Y211 samples processed under similar conditions. Although similar processes are used, depending upon the crystal structure and the lattice mismatch, the nanocolumns in YBCO can form that influence the high field J_c .

REFERENCES

1. D. Larbalestier, A. Gurevich, D. M. Feldmann, A. Polyanski, "High- T_c superconducting materials for electric power applications," *Nature*, vol. 414, pp. 368-377, 2001
2. T. J. Haugan, P. N. Barnes, R. Wheeler, F. Meisenkothen, M. Sumption, "Addition of nanoparticle dispersions to enhance flux pinning of the $YBa_2Cu_3O_{7-x}$ superconductor," *Nature*, vol. 430, pp. 867-870, 2004
3. C. Varanasi, P. N. Barnes, J. Burke, J. Carpenter, T. J. Haugan, "Controlled introduction of flux pinning centers in $YBa_2Cu_3O_{7-x}$ films during pulsed-laser deposition," *Appl. Phys. Lett.*, vol. 87, pp. 262510-12, 2005
4. T. A. Campbell, T. J. Haugan, I. Maartense, J. Murphy, L. Brunke, P. Barnes, "Flux pinning effects of Y_2O_3 nanoparticle dispersions in multilayered YBCO thin films" *Physica C*, vol. 423, pp.1-8, 2005
5. J. L. MacManus-Driscoll, S. R. Foltyn, Q. X. Jia, H. Wang, A. Serquis, L. Civale, B. Maiorov, M. E. Hawley, M. P. Maley, D. E. Peterson, "Strongly enhanced current densities in superconducting coated conductors of $YBa_2Cu_3O_{7-x} + BaZrO_3$," *Nature Materials*, vol. 3, pp. 439-441, 2004
6. C. V. Varanasi, P. N. Barnes, J. Burke, L. Brunke, I. Maartense, T. J. Haugan, E. A. Stinzianni, K. A. Dunn, P. Haldar, "Flux pinning enhancement in $YBa_2Cu_3O_{7-x}$ films with $BaSnO_3$ nanoparticles," *Supercond. Sci. Technol.* vol.19, pp.L37-L41, 2006
7. S. Kang, A. Goyal, J. Li A.A. Gapud, P.M. Martin, L. Heatherly, J.R. Thomson, D.K. Christen, F.A. List, M. Paranthaman, D.F. Lee, "High-performance high- T_c superconducting wires" *Science* vol. 311, pp.1911-1914, 2006
8. P. Mele, K. Matsumoto, T. Horide, A. Ichinose, M. Mukaida, Y. Yoshida, S. Horii, "Insertion of nanoparticulate artificial pinning centers in $YBa_2Cu_3O_{7-x}$ films by laser ablation of a Y_2O_3 -surface modified target" *Supercond. Sci. Technol.* vol.20, pp. 616-620, 2007
9. C.V. Varanasi, J. Burke, L. Brunke, H. Wang, M. Sumption, P.N. Barnes, "Enhancement and angular dependence of transport critical current density in pulsed laser deposited $YBa_2Cu_3O_{7-x}+BaSnO_3$ films in applied magnetic fields" *J. Appl. Phys.* vol. 102, pp.063909-1-5, 2007
10. C. V. Varanasi, P.N. Barnes, J. Burke, "Enhanced flux pinning force and uniquely shaped flux pinning force plots observed in $YBa_2Cu_3O_{7-x}$ films with $BaSnO_3$ nanoparticles" *Supercond. Sci. Technol.* vol. 20 pp.1071-1075, 2007
11. R.L.S. Emergo, J. Z. Wu, T.J. Haugan, P.N. Barnes, "Tuning porosity of $YBa_2Cu_3O_{7-8}$ vicinal films by insertion of Y_2BaCuO_5 nanoparticles" *Appl.Phys.Lett.*87, pp. 232503-1-3, 2005
12. A. Goyal, S. Kang, K.J. Leonard, P.M. Martin, A.A. Gapud, M. Varela, M. Paranthaman, A.O. Ijaluola, E.D. Specht, J.R. Thomson, D.K. Christen, S.J. Pennycook, F.A. List, "Irradiation-free, columnar defects comprised of self-assembled nanodots and nanorods resulting in strongly enhanced flux-pinning in $YBa_2Cu_3O_{7-8}$ films" *Supercond. Sci. Technol.* vol. 18, pp.1533-1538, 2005
13. J.P. Rodriguez, P.N. Barnes, C.V. Varanasi, "In- field current of type-II superconductors caused by strain from Nanoscale columnar inclusions" *Phys. Rev. B* vol.78, pp. 052505-1-4, 2008